Earth's inner core: Innermost inner core or hemispherical variations?

K.H. Lythgoe [a,*], A. Deuss [a], J.F. Rudge [a], J.A. Neufeld [a,b,c]

[a] *Bullard Laboratories, Department of Earth Sciences, Madingley Road, Cambridge, CB3 0EZ, UK*
[b] *BP Institute, Madingley Road, Cambridge, CB3 0EZ, UK*
[c] *Department of Applied Mathematics and Theoretical Physics, Centre for Mathematical Sciences, Wilberforce Road, Cambridge, CB3 0WA, UK*

A B S T R A C T

The structure of Earth's deep inner core has important implications for core evolution, since it is thought to be related to the early stages of core formation. Previous studies have suggested that there exists an innermost inner core with distinct anisotropy relative to the rest of the inner core. Using an extensive new data set of handpicked absolute travel time observations of the inner core phase PKIKP, we find that the data are best explained by variations in anisotropy between two hemispheres and do not require an innermost inner core. We demonstrate that observations of an innermost inner core are an artifact from averaging over lateral anisotropy variations. More significantly we show that hemispherical variations in anisotropy, previously only imaged in the upper inner core, continue to its centre. The eastern region has 0.5–1.5% anisotropy, whereas the western region has 3.5–8.8% anisotropy increasing with depth, with a slow direction at 57–61° to the Earth's rotation axis at all depths. Such anisotropy is consistent with models of aligned hcp or bcc iron aggregates.

© 2013 Elsevier B.V. All rights reserved.

1. Introduction

Since velocity anisotropy in the inner core was first proposed (Morelli et al., 1986; Woodhouse et al., 1986), with a fast direction parallel to Earth's rotation axis and a slow direction perpendicular to it, reports of increasing complexity in the structure of the inner core have continued. Degree 1 lateral variations in anisotropy have been imaged with both body waves (Tanaka and Hamaguchi, 1997; Creager, 1999; Niu and Wen, 2001; Garcia, 2002; Waszek et al., 2011; Irving and Deuss, 2011) and normal modes (Deuss et al., 2010). The western 'hemisphere' has stronger anisotropy than the eastern, and also appears to be slower, at least in the upper 100 km (Niu and Wen, 2001; Wen and Niu, 2002; Waszek et al., 2011). Hemispheres have been imaged up to 600–700 km below the inner core boundary (Creager, 1999; Sun and Song, 2008; Irving and Deuss, 2011; Tanaka, 2012), although there is some disagreement about the exact location of hemisphere boundaries.

More recently, a region of distinct anisotropy at the centre of the inner core has been reported (Ishii and Dziewonski, 2002). This apparent innermost inner core (IMIC) has greater anisotropy than the rest of the inner core and a slow direction that is no longer perpendicular to Earth's rotation axis. However, there is no consistent image of the IMIC, with its radius and slow direction differing between models (Ishii and Dziewonski, 2002;

Beghein and Trampert, 2003; Cormier and Stroujkova, 2005; Cao and Romanowicz, 2007; Sun and Song, 2008; Niu and Chen, 2008).

Ishii and Dziewonski (2002) originally suggested the existence of an IMIC, with a radius of 300 km and a slow direction at 45° to Earth's rotation axis. Using normal mode splitting, Beghein and Trampert (2003) subsequently updated the IMIC radius to 400 km and the slow direction to being parallel to Earth's spin axis. Waveform analysis by Cormier and Stroujkova (2005) found no evidence for a sharp IMIC and concluded that if an IMIC were to exist it would need to have a radius of at least 500 km, with a transition region of at least 100 km. Cao and Romanowicz (2007) reported that if an IMIC is present, it most likely has a radius of 500 km and a slowest direction at 55° to Earth's rotation axis. Lastly, Sun and Song (2008) find an IMIC radius of 590 km, although their study cannot be used to test for its existence, since an IMIC is hard-wired into the model.

Here we present a new, high quality body wave data set and use it to study anisotropy in the deep inner core. Specifically we investigate the depth extent of hemispherical variations and test if the existence of an innermost inner core is actually required by the seismic data.

2. Data and methods

We use the inner core compressional body wave phase, PKIKP, to investigate the deep inner core, since normal modes have no sensitivity to the centre of the Earth and are unable to image sharp boundaries. Many previous inner core studies have measured
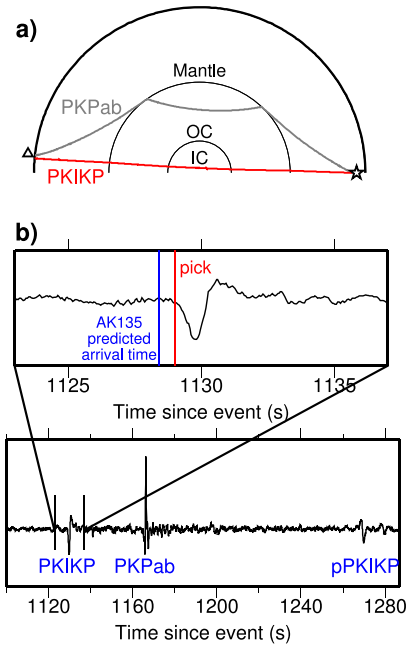

Fig. 1. (a) Ray paths of PKIKP (red) and PKPab (grey) through the Earth for an event–receiver epicentral distance of 180°. (b) Example seismogram, showing the PKIKP arrival and predicted arrival time for AK135. Seismogram is for an event on 22nd September 2006 in Argentina (M_w6) recorded at HIA station in northern China. (For interpretation of the references to colour in this figure legend, the reader is referred to the web version of this article.)

the arrival time of PKIKP – which travels through the mantle, outer and inner core (Fig. 1a) – with respect to a reference phase traversing only the mantle and outer core (PKPbc or PKPab), in order to remove the effect of mantle heterogeneity and source mislocation (Creager, 1999; Irving and Deuss, 2011). PKPbc arrives at epicentral distances less than 155.5°, so PKPbc–PKIKP data is only sensitive to the upper 350 km of the inner core. Additionally at large epicentral distances (hence large inner core depths) PKIKP and the reference phase, PKPab, have very different paths in the mantle and so differences in travel time between the two phases cannot be attributed to the inner core alone. We therefore study absolute travel times of PKIKP, without a reference phase. Past studies of absolute PKIKP travel times have used data from the International Seismological Centre (Ishii and Dziewonski, 2002; Su and Dziewonski, 1995), which despite being a large data set is noisy and may miss anomalous arrivals. Therefore, we prefer to use our own handpicked measurements to ensure that our data set is of the highest quality.

We have assembled a data set of ~2360 high-quality, hand-picked absolute PKIKP arrival times, the largest yet used to study the inner core. We use events with a moment magnitude (M_w) greater than 6 for the time period 1990–2008, for which the EHB catalogue (Engdahl et al., 1998) is available, providing accurate relocated event hypocentres and origin times. When targeting polar paths, we lowered the magnitude threshold to $M_w > 5$ in order to obtain more data. To ensure that PKIKP can be easily identified, source–receiver epicentral distances of 150–180° are used, corresponding to ray turning depths of less than 1010 km radius. We pick the onset of PKIKP arrivals and so are unaffected by waveform broadening due to inner core attenuation.

The arrival time of PKIKP is measured with respect to the predicted arrival time from the 1D Earth model AK135 (Fig. 1b; Kennett et al., 1995) and is corrected for ellipticity (Dziewonski and Gilbert, 1976). To reduce the effect of mantle heterogeneity, we apply mantle corrections using a global P-wave model

(Li et al., 2008). Since PKIKP travels vertically in the mantle, relatively little travel time signature is obtained from the mantle. We also compare our results for the top of the inner core to differential travel time studies, where the studied region overlaps, to confirm that there is minimal mantle influence. We assume that the outer core is seismically homogeneous, since it is vigorously convecting and previous seismic studies have found no heterogeneity (Souriau et al., 2003; Ishii and Dziewonski, 2005).

We investigate anisotropy by analysing travel time as a function of ray angle with Earth's rotation axis in the inner core. Following Creager (1992), we parametrise weak cylindrical anisotropy as a perturbation to a spherically symmetric model by

$$\frac{\delta t}{t} = -\frac{\delta v}{v} = a + b\cos^2 \zeta + c\cos^4 \zeta, \tag{1}$$

where v is the P-wave velocity in the reference model, δv is the velocity perturbation, t is the time the ray spends in the inner core, δt is our measured travel time residual and ζ is the angle between the ray path in the inner core and Earth's rotation axis. In this form a represents the difference between the observed equatorial velocity and the reference model and b and c describe the anisotropic variation of travel time with ζ. We define rays with $\zeta \leqslant 35°$ as polar rays and $\zeta > 35°$ as equatorial rays.

The total anisotropy (δv_{ani}) is defined as the difference between purely polar ($\zeta = 0°$) and purely equatorial ($\zeta = 90°$) rays, i.e.

$$\delta v_{ani} = b + c, \tag{2}$$

while the average isotropic velocity perturbation (δv_{iso}) is found by averaging over all ray angles

$$\delta v_{iso} = a + \frac{b}{3} + \frac{c}{5}. \tag{3}$$

We invert our observed travel times (δt) for parameters a, b and c from Eq. (1), using a linear least squares inversion without damping. We parametrise the model into discrete layers in order to avoid smoothing any depth variations and trace the rays through the layers and hemispheres to obtain the anisotropic and isotropic perturbations for each layer and hemisphere.

Earlier studies of inner core hemispherical variations have attributed a ray's travel time anomaly to one hemisphere only, based on the turning location of the ray (Tanaka and Hamaguchi, 1997; Creager, 1999; Niu and Wen, 2001; Garcia, 2002; Waszek et al., 2011; Irving and Deuss, 2011). However this method does not account for time the ray has spent in the other hemisphere, which becomes more important at depth since ray paths are long and tend to travel through both hemispheres. Therefore our tomographic ray tracing technique is more precise in resolving lateral variations, especially at depth, since we correctly attribute parts of each ray to the corresponding hemisphere.

Sun and Song (2008) applied body wave tomography of the inner core to PKP differential travel times. However the model of Sun and Song (2008) cannot be used to investigate the existence of an IMIC since its radius is defined a priori, along with the location of hemisphere boundaries. Here, we vary the location of the boundaries to find the solution that best fits the data. Differential travel times are also known to become increasingly unreliable as epicentral distance – hence inner core depth – increases, because the reference phase PKPab spends more time in the strongly heterogeneous D″ layer. As part of their study, Sun and Song (2008) investigate the difference between their quasi-3D method and a 1D ray tracing method and find very little difference between the two approaches.

Anisotropy in the IMIC has been defined as having a slowest direction which is no longer in the equatorial plane ($\zeta_{slow} = 90°$), with estimated slow angles (ζ_{slow}) ranging from 0° (Beghein and

Trampert, 2003) to 55° (Cao and Romanowicz, 2007) from the rotation axis, with other intermediate values (Ishii and Dziewonski, 2002; Sun and Song, 2008). These earlier studies visually assessed the slowest direction, but we quantify it analytically by finding the maximum of Eq. (1). We do this by differentiating Eq. (1) with respect to ζ

$$\frac{d(\delta t/t)}{d\zeta} = -2\cos(\zeta)\sin(\zeta)\big(b + 2c\cos^2(\zeta)\big) \qquad (4)$$

which is zero at

$$\zeta_{\text{slow}} = \cos^{-1}\sqrt{\frac{-b}{2c}}. \qquad (5)$$

We quantify how significant this slow direction is by subtracting the model predicted travel time residual at the slowest angle from the predicted travel time residual for a purely equatorial ray ($\zeta = 90°$).

We use an L2 misfit to assess how well the model matches our data

$$L2 = \frac{1}{N}\sum_{i=1}^{N}(\delta t_{\text{obs}} - \delta t_{\text{pred}})_i^2 \qquad (6)$$

where N is the number of rays, δt_{obs} is the observed travel time residual and δt_{pred} is the model predicted travel time residual. Model uncertainties have been estimated from cross-validation, whereby a random 10% of the data is removed and a new model obtained. This is repeated 10 times with a different data subset removed each time, such that each data point is absent from one model. We compare the resulting 10 models to the initial model in order to quantitatively measure model fit and uncertainty.

We also want to compare our observed seismological anisotropy to predicted anisotropy for mineral physics models of iron at inner core conditions. These models are quantified by the elastic parameters C_{ij}. Following Mattesini et al. (2010) and Stixrude and Cohen (1995), P-wave velocity for a single crystal of hcp iron with cylindrical symmetry, or for a bcc aggregate with symmetry axis at (1 1 1), can be expressed as

$$v_{\text{p}} = \bigg(\frac{1}{\rho}\big(C_{11} + (4C_{44} + 2C_{13} - 2C_{11})\cos^2(\zeta)$$
$$+ (C_{33} + C_{11} - 4C_{44} - 2C_{13})\cos^4(\zeta)\big)\bigg)^{\frac{1}{2}}. \qquad (7)$$

where ρ is density. Eq. (7) is valid for hexagonal close-packed (hcp) iron with cylindrical symmetry or for a body-centred-cubic (bcc) aggregate with symmetry axis at (1 1 1). Assuming that all crystals are aligned in one direction, the travel time residual can be approximated by

$$\frac{\delta t}{t} = -\frac{\delta v_{\text{p}}}{v_{\text{p0}}} \qquad (8)$$

where v_{p0} is the Voigt average velocity and $\delta v_{\text{p}} = v_{\text{p}} - v_{\text{p0}}$.

3. Results

Our data set has good global coverage, with ~2250 equatorial paths ($\zeta > 35°$, Fig. 2a) and ~110 polar paths ($\zeta \leqslant 35°$, Fig. 2b). Unlike differential travel time studies, our polar paths are not dominated by South Sandwich Island events. Equatorial travel time residuals range from −2 to 6 s (Figs. 2a, 2c) and so arrive late on average, indicating that equatorial rays generally travel slower than predicted by AK135. Conversely polar residuals range from −9 to 4 s (Figs. 2b, 2d), so polar rays generally travel faster than predicted by AK135. Polar paths also display large longitudinal variations, with anomalously fast polar paths travelling the inner core between approximately 150°W and 40°E longitude (Fig. 2d).

We firstly examine global inner core anisotropy without allowing for hemispherical variations (Fig. 3). Our whole data set as a function of ζ is shown in Fig. 3a. Figs. 3b and 3c show the model resulting from the inversion for an inner core separated into three depth layers, with boundaries at 750 km and 550 km radius. Allowing for global anisotropy reduces our model misfit by 34% (Table 1) compared to no anisotropy. The model explains the data well for each layer (Figs. 3d–3f), with the resulting a, b and c values given in Table 1.

We find that anisotropy increases with depth, from around 2% at the top of the inner core to over 5% in the centre (Fig. 3b). The predicted anisotropy curves (i.e. Eq. (1)) for the top two layers (blue curves, Fig. 3g) show cylindrical anisotropy, with polar rays travelling faster than equatorial rays. However at a radius of less than 550 km (orange curve, Fig. 3g) the form of anisotropy changes to having a slowest angle at ~56° to the rotation axis (Fig. 3h). The slowest angle becomes more 'significant' the more its travel time residual differs from that in the equatorial direction, thus the slow angle of the top two layers is 'insignificant', while the bottom layer is 'significant' (Fig. 3i).

Anisotropy also increases with depth using a polynomial depth parametrisation, but there is less constraint on the depth at which the form of anisotropy changes. We have varied the thickness of the deepest layer in our inversion and found the thickness of the apparent IMIC to be 550 ± 50 km. The base of the top layer at a radius of 750 km is effectively arbitrary but is chosen to equally distribute data across the three layers and demonstrates that anisotropy increases gradually with depth. Comparing our results with previous studies, we find that our laterally-averaged

Table 1

a, b and c values in each depth layer for three models: without anisotropy and hemispherical variations; with anisotropy but without hemispherical variations; with anisotropy and hemispherical variations. Misfits for each model are also given.

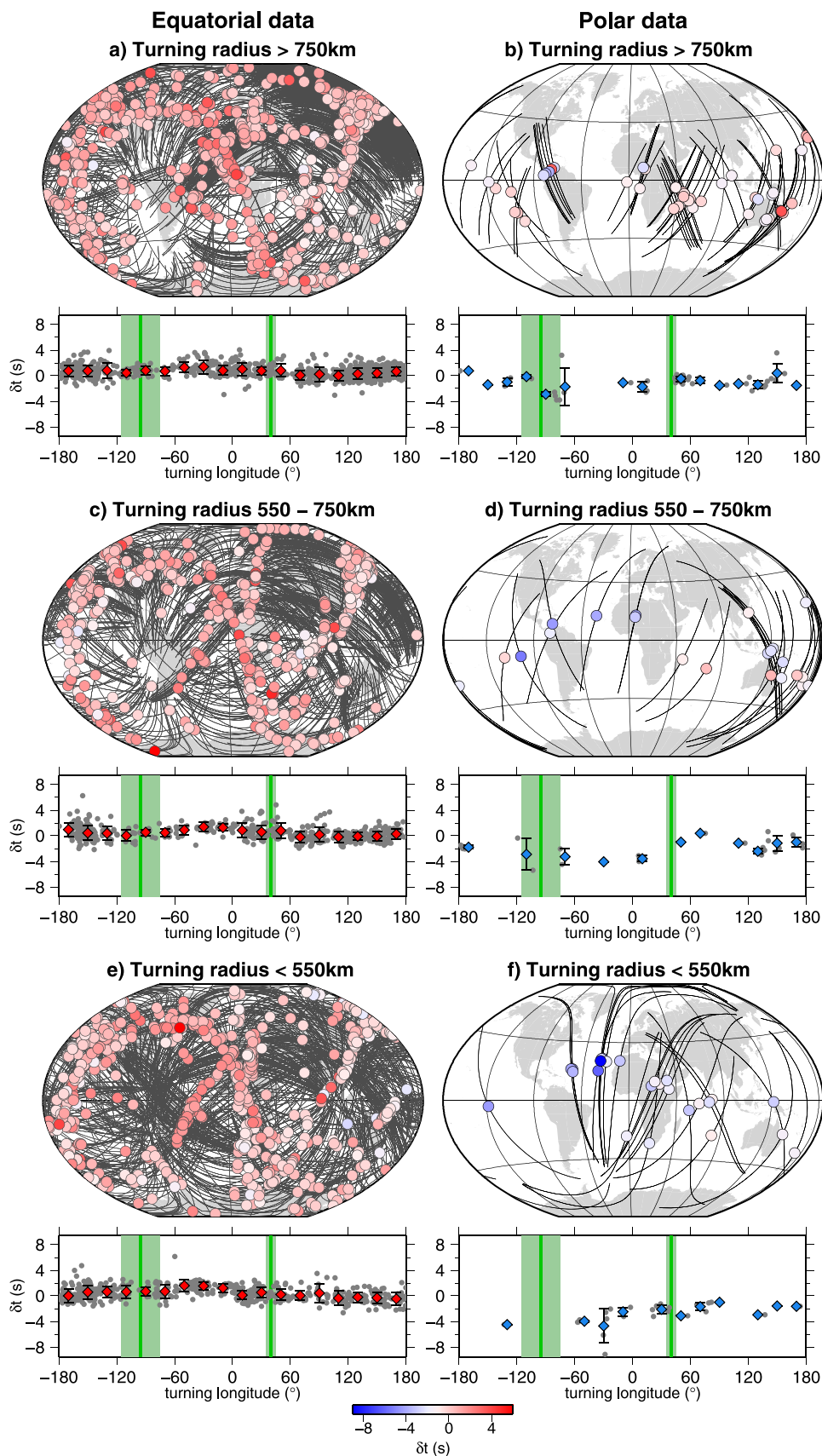| Model	Radius	a	b	c	Misfit (s^2)
No anisotropy		0	0	0	1.43
Anisotropy	>750 km	−0.0048	−0.0036	0.0215	0.95
	750–550 km	−0.0008	−0.0089	0.0420	
	<550 km	0.0070	−0.0950	0.1503	
Hemispheres					
East	>750 km	−0.0043	0.0040	0.0099	0.81
	750–550 km	−0.0025	0.0336	−0.0220	
	<550 km	0.0060	−0.0213	0.0264	
West	>750 km	−0.0062	−0.0308	0.0658	
	750–550 km	0.0049	−0.0836	0.1423	
	<550 km	0.0067	−0.1318	0.2194	

Fig. 2. PKIKP travel time residuals, corrected for ellipticity and mantle heterogeneity, for equatorial (a, c, e) and polar paths (b, d, f) and separated according to ray turning point radius: greater than 750 km radius (a, b); between 550 km and 750 km radius (c, d); less than 550 km radius (e, f). Top panels show residuals in map form, plotted at the turning point with inner core ray paths plotted as black lines. Bottom panels show residuals as a function of turning point longitude (grey dots). Red/blue diamonds show average residuals over 20° longitude bins, with error bars plotted as one standard deviation. Green lines show minimum misfit hemisphere boundary locations from Fig. 4 with shading for cross-validation errors. (For interpretation of the references to colour in this figure legend, the reader is referred to the web version of this article.)
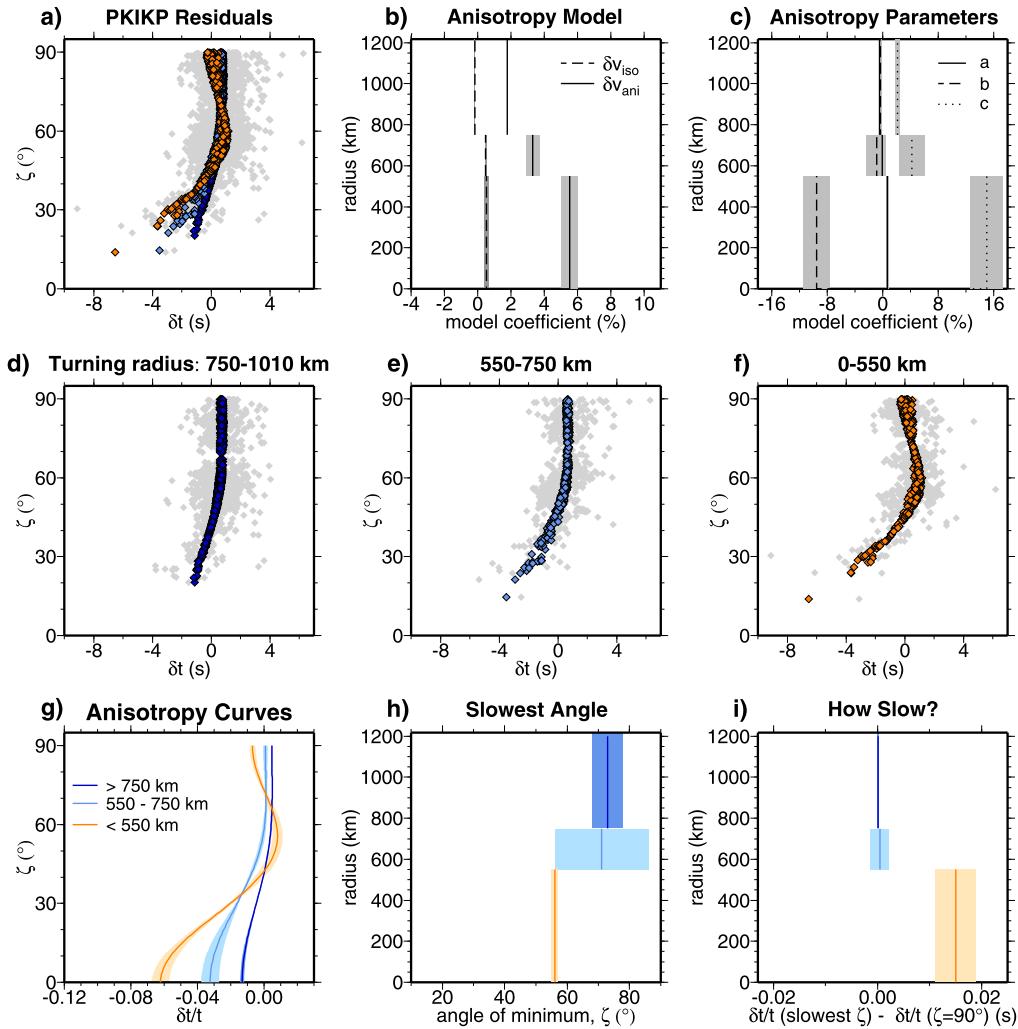
Fig. 3. Results of inversion without allowing for hemispherical variations. (a) Observed PKIKP travel time residuals (grey) with model predicted travel time residuals, coloured corresponding to ray turning depth: dark blue = turning in top layer, light blue = turning in middle layer, red = turning in bottom layer. (b) Isotropic (dashed) and anisotropic (solid line) variations with respect to AK135. (c) Model values for *a*, *b* and *c* (Eq. (1)). Observed residuals (grey) and model predicted residuals (dark blue) for rays that turn between (d) 750–1010 km radius, (e) 550–750 km radius and (f) less than 550 km radius. (g) Anisotropy curves for $\delta t/t$ in each layer. (h) ζ for which the anisotropy curve is maximum (the slowest angle). (i) Difference between $\delta t/t$ for the slowest angle and the equatorial direction ($\zeta = 90°$). Shaded regions show errors obtained by cross-validation. (For interpretation of the references to colour in this figure legend, the reader is referred to the web version of this article.)

model is consistent with the presence of an IMIC at 550 km radius (Cormier and Stroujkova, 2005; Cao and Romanowicz, 2007).

However previous IMIC studies have not accounted for hemispherical variations, which have been extensively imaged in the upper inner core. We would like to investigate if these two properties can be reconciled. We again invert our data for parameters *a*, *b* and *c* (Eq. (1)) for 3 layers, but now allowing for variation between two hemispheres. The location of the hemisphere boundaries is varied systematically in a grid search, in order to find the boundaries with the lowest misfit (Fig. 4a). The best-fitting boundaries are at −95°W and 40°E, with a further misfit reduction of 15% compared to the model with no hemispherical variations (Table 1). We also perform a statistical F-test and conclude that this misfit reduction is significant, at 99% confidence level, given the increased number of model parameters.

The location of the eastern boundary is consistent with that of all previous studies (Fig. 4b; Tanaka and Hamaguchi, 1997; Creager, 1999; Garcia, 2002; Niu and Wen, 2001; Waszek et al., 2011; Irving and Deuss, 2011), while the western boundary is located further eastwards than other studies have observed (Fig. 4c). However it should be noted that past studies are only sensitive to the upper inner core (≥600 km radius). Although there is some

variation in the travel time residual of polar paths between −95° and −150° (Fig. 2d), most paths are not anomalous and so the anisotropy boundary is placed at −95° and not further westwards. This explains why the western boundary has a broad minimum with a higher uncertainty and indicates several possibilities: that the boundary is not sharp, has some depth variability or that it cannot be resolved accurately with present data coverage.

Fig. 5 shows the resulting models for the eastern and western hemispheres, using the same layered parametrisation as in our global model (Fig. 3) and the lowest misfit boundary locations (Fig. 4). Anisotropy throughout the entire eastern hemisphere is small, ranging from 0.5 to 1.5%, with little variation of travel time with ray angle in any layer (Figs. 5a–5c). The slight variation that does exist is very small, especially given errors in the inversion. The eastern hemisphere generally has a slowest angle at 90° to the rotation axis (Fig. 5d). The bottom layer has a slow direction at 51° to the rotation axis, but has a large associated error (±13°) and there is only a very small difference between $\delta t/t$ for the slowest angle and 90° (Fig. 5e).

Conversely the western hemisphere has large anisotropy that increases with depth, from 3.5% in the top layer to 8.8% in the deepest layer (Figs. 5f–5h). A slow direction at 57–61° is seen
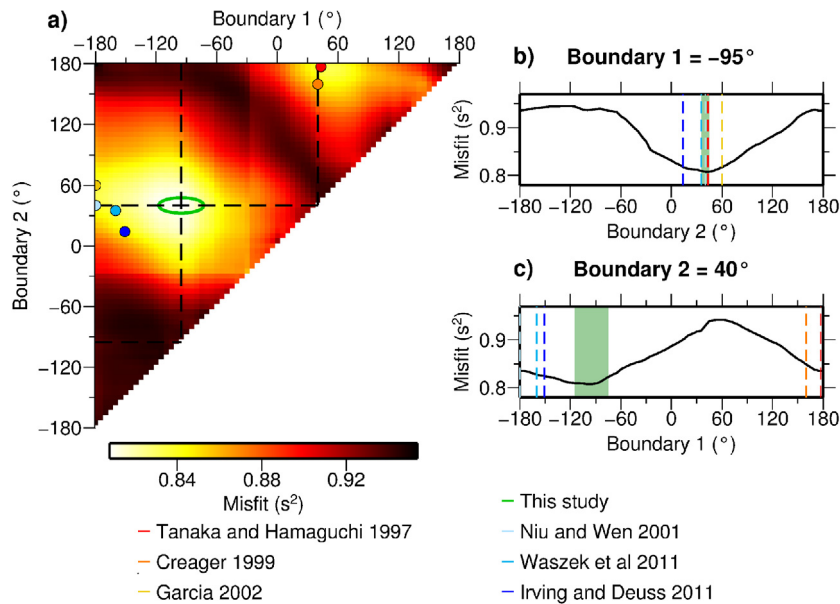
Fig. 4. (a) Misfit contour plot of boundary locations. Minimum misfit is at $40 \pm 5°E$ and $95 \pm 20°W$, with the error range marked by the green ellipse. (b, c) Cross-section through minimum misfit boundary locations. Boundary locations are also plotted from previous studies.

throughout the western hemisphere (Fig. 5i), but slowness appears to become more significant with depth as anisotropy increases (Fig. 5j). Hence, a slowest direction at intermediate angles is already present for a radius larger than 550 km and we do not require the presence of an innermost inner core. It should be noted that the sharp changes with depth seen in the western hemisphere are artifacts of inverting for discrete layers and it is likely that the increase in anisotropy is smoother.

To exclude any bias in the upper layers from rays travelling through the central layer, the same inversion is performed using short distance data that sample the top two layers only. In this instance anisotropy in the top layers doesn't change, showing that the stronger anomalies of deeper ray paths do not influence the upper layers. Moving the western boundary towards $-180°$, to be consistent with previous studies, also has little effect on the resulting anisotropy model, because the western boundary is only constrained by a few polar paths. The hemisphere model still has the lowest misfit and again there is no need for an innermost inner core.

4. Discussion

4.1. Innermost inner core versus hemispherical variations

A change in slow direction from $90°$ to an intermediate angle in the deep inner core, was previously thought to be evidence of an IMIC (Fig. 6a; Ishii and Dziewonski, 2002). However no past studies accounted for hemispherical variations and therefore averaged over eastern and western hemispheres. At greater depths, ray paths are longer and tend to travel through both hemispheres, so the change in slow direction becomes apparent in the averaged model at depth, as seen in Fig. 3. This may explain why different studies find differing IMIC depths. Consequently by properly accounting for hemispherical variations we find no evidence for an IMIC and, more significantly, we show that hemispheres continue to the centre of the Earth (see Fig. 6b for a schematic of hemispherical structure). Therefore we demonstrate that the IMIC is an artifact from averaging over the two hemispheres.

Isotropic velocities in our models are similar to AK135 in both hemispheres, implying that the hemispheres have a similar composition. Hemispherical differences arise from anisotropy and we

show that anisotropy is confined to a western hemisphere 'wedge' between $-95°W$ and $40°E$. However the sharpness of hemisphere boundaries, particularly the western boundary, cannot be accurately resolved with present data coverage, since there are few polar paths in this region.

Since we are studying travel times, we have no constraints on attenuation and do not exclude a change in attenuation with depth, as seen by Cormier and Li (2002) and Li and Cormier (2002). Although Li and Cormier (2002) found no obvious hemispherical differences in attenuation, this should be analysed further since the change in attenuation with depth may be confined to one hemisphere only.

4.2. Interpretation

We have found that the slowest direction at intermediate angles is a feature of the whole western hemisphere and is not confined to an IMIC. We now want to see if this form of anisotropy is consistent with predictions from mineral physics. To do this, we calculate the predicted seismic anisotropy curves for several mineral physical models of iron at inner core conditions using Eq. (7) and assuming that all hcp crystals are aligned in one direction. In Fig. 7 we compare our observed seismic anisotropy to models of hcp iron aggregates with the fast axis aligned with Earth's spin axis (Stixrude and Cohen, 1995; Steinle-Neumann et al., 2001; Vocadlo et al., 2009; Mattesini et al., 2010; Sha and Cohen, 2010; Martorell et al., 2013) and a model of a cylindrically averaged bcc iron aggregate with 25% of its [111] axes aligned with the spin axis (Mattesini et al., 2010). For most hcp models the [001] axis is fastest (Stixrude and Cohen, 1995; Mattesini et al., 2010; Sha and Cohen, 2010; Martorell et al., 2013), so this axis is aligned along Earth's spin axis. However for some hcp models this axis is slow and therefore has been rotated to lie in the equatorial plane (i.e. for models by Steinle-Neumann et al., 2001; Vocadlo et al., 2009).

All mineral physics models predict some anisotropy, so are inconsistent with the small amount of observed eastern hemisphere anisotropy. Significantly all models predict a slowest direction at intermediate angles – ranging from $49°$ to $59°$ to the rotation axis (Mattesini et al., 2010; Steinle-Neumann et al., 2001) – and so qualitatively match western hemisphere anisotropy (Fig. 7).
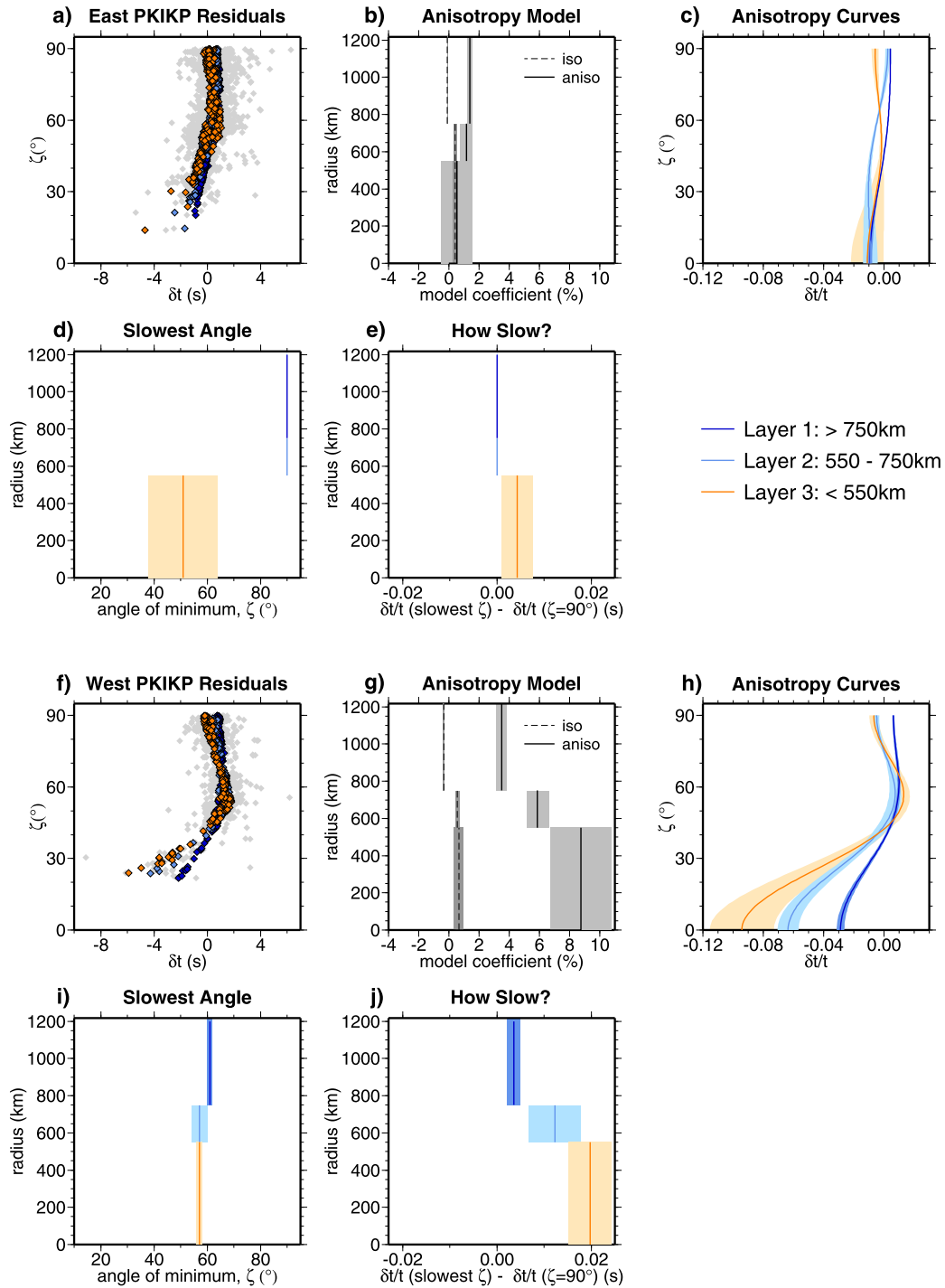
Fig. 5. Anisotropy model for eastern (top) and western (bottom) hemispheres with hemisphere boundaries at 95°W and 40°E, and radial boundaries at 750 km and 550 km. (a) Observed PKIKP travel time residuals (grey) and model predicted travel time residuals (colour) plotted for data with a turning position in the eastern hemisphere. (b) Eastern hemisphere model isotropic (dashed) and anisotropic (solid) variations with respect to AK135. (c) Anisotropy curves for eastern hemisphere. (d) ζ for which the anisotropy curve is maximum. (e) Difference between $\delta t/t$ for the slowest angle and the equatorial direction ($\zeta = 90°$). (f–j) for the western hemisphere. Shaded regions show errors obtained from cross-validation. (For interpretation of the references to colour in this figure legend, the reader is referred to the web version of this article.)

In the western hemisphere, most models underestimate the difference between equatorial and polar velocities (Stixrude and Cohen, 1995; Vocadlo et al., 2009; Mattesini et al., 2010; Sha and Cohen, 2010; Martorell et al., 2013). The models of Stixrude and Cohen (1995) and Steinle-Neumann et al. (2001) have slow directions at 56° and 59° to the rotation axis respectively, matching the seismically observed slow direction. bcc iron (Mattesini et al., 2010) matches deep anisotropy for polar angles, but not for equatorial angles. The model of Steinle-Neumann et al. (2001) is the only model to predict sufficient anisotropy to match the seismic observations.

There is much variation between published mineral physics models, with no model completely matching seismically observed anisotropy. This is unsurprising given the difficulty in recreating the conditions of the inner core – all models are at incorrect pressures or temperatures and light elements are not accounted for.
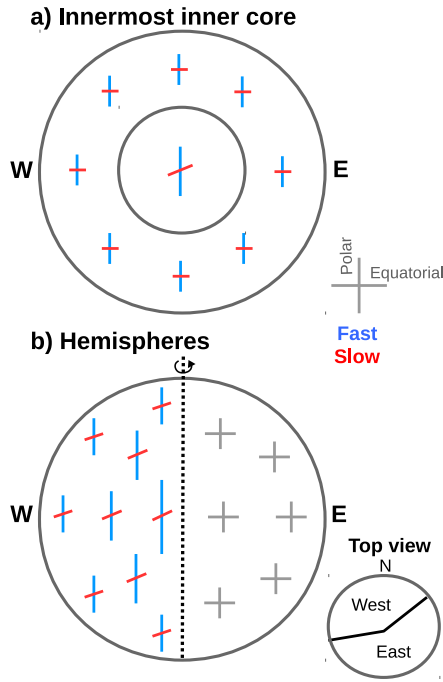
a) Innermost inner core

b) Hemispheres

Fig. 6. Schematic of inner core models with either (a) an innermost inner core which has larger anisotropy and a slow direction at ∼56° to the rotation axis or (b) hemispherical variations where the eastern hemisphere is weakly anisotropic and the western hemisphere has high anisotropy that increases with depth, with a slow direction at 57–61° throughout. Blue and red lines represent the fast and slow directions respectively. The length of the fast direction corresponds to the magnitude of anisotropy. (For interpretation of the references to colour in this figure legend, the reader is referred to the web version of this article.)

It is also reasonable to assume that texturing in the inner core is more complex than we analyse here. Nevertheless, all models

agree on the slowest angle not being perpendicular to the rotation axis.

Since all iron models are qualitatively consistent with western hemisphere anisotropy, this implies that the western hemisphere is textured, with crystals oriented along Earth's rotation axis. Increasing anisotropy with depth implies that the degree of texturing also increases. Conversely eastern hemisphere anisotropy shows no correlation with any model, suggesting that crystals are randomly aligned. We must therefore look for a mechanism that will generate a wedge of aligned crystals with a longitude width of ∼135° and with the degree of alignment increasing with depth.

Translation of the inner core, whereby the whole inner core moves in one direction resulting in melting and crystallisation on opposite sides, is one proposed mechanism (Monnereau et al., 2010; Alboussiere et al., 2010). However many parts of this mechanism are unclear, primarily the actual process that causes crystals to align. Furthermore translation requires a high inner core viscosity which is relatively unconstrained, with possible values varying by several orders of magnitude. Recent estimates of core thermal conductivity are high (Pozzo et al., 2012) and so for translation to occur it must be compositionally rather than thermally driven (Deguen et al., 2013; Gubbins et al., 2013).

Alternatively variations in heat flow at the core–mantle boundary from mantle convection, may extend to the inner core boundary (ICB) causing heterogeneous crystallisation rates (Aubert et al., 2011), and even melting (Gubbins et al., 2011). Calkins et al. (2012) recently showed that topography at the core–mantle boundary could cause significant longitudinal variations in heat flow along the ICB. These mechanism requires textural development from solidification processes, such as alignment with Earth's magnetic field (Karato, 1993) or dendritic solidification (Bergman, 1997). Yoshida et al. (1996) propose that anisotropy develops from topographic relaxation due to differential crystallisation rates between the equator and pole. If crystallisation rates vary in localised regions, this could feasibly generate localised regions of anisotropy.
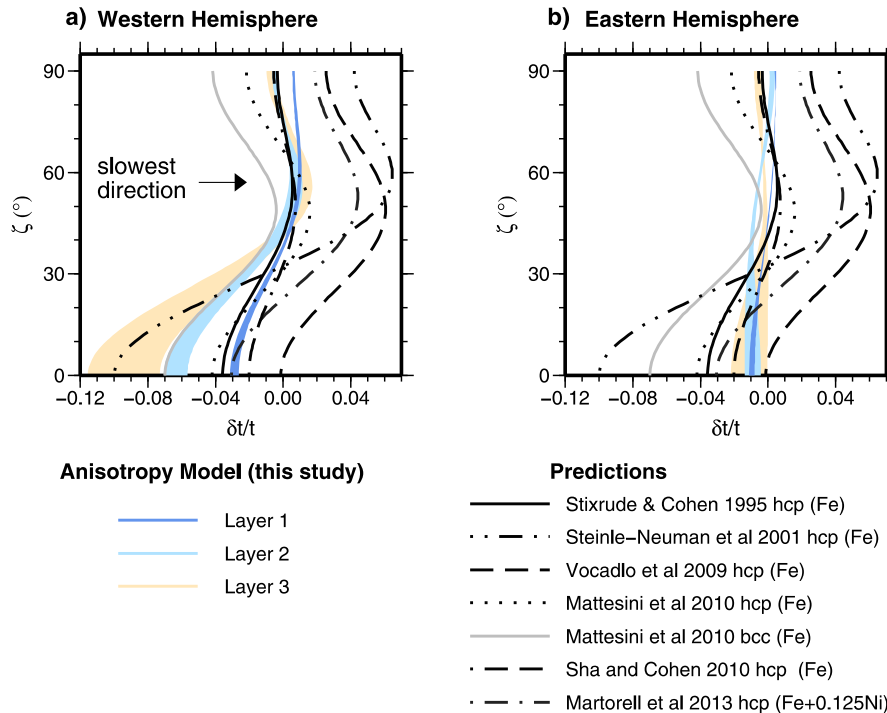

Fig. 7. Anisotropy curves for (a) western and (b) eastern hemispheres. The anisotropy model from this study is plotted as in Figs. 5c and 5h, with layer 1 above 750 km (dark blue), layer 2 from 550 to 750 km (light blue) and layer 3 below 550 km (orange). Also plotted are predicted anisotropy curves for different iron models at inner core conditions. (For interpretation of the references to colour in this figure legend, the reader is referred to the web version of this article.)

5. Conclusions

Using our extensive new data set of PKIKP travel time observations, we show that hemispherical variations extend throughout the entire inner core, with a strongly anisotropic western hemisphere and a weakly anisotropic eastern. A slow direction at 57–61° is seen throughout the western hemisphere and is also required in models of bcc and hcp iron at core conditions. However there is significant variation between mineral physics models and no model provides a complete match to our seismic observations. We further show that previous observations of an innermost inner core at the centre of the Earth result from averaging over lateral variations and that an innermost inner core is not required by our data. Our observation of distinct hemispheres at all depths poses an intriguing problem: how to generate degree 1 asymmetry throughout the entire inner core.

Acknowledgements

References

Alboussiere, T., Deguen, R., Melzani, M., 2010. Melting-induced stratification above the Earth's inner core due to convective translation. Nature 2466, 744–747.

Aubert, J., Amit, H., Hulot, G., Olson, P., 2011. Thermochemical flows couple the Earth's inner core growth to mantle heterogeneity. Nature 454, 758–761.

Beghein, C., Trampert, J., 2003. Robust normal mode constraints on inner core anisotropy from model space search. Science 299, 552–555.

Bergman, M.I., 1997. Measurements of elastic anisotropy due to solidification texturing and the implications for the Earth's inner core. Nature 389, 60–63.

Calkins, M.A., Noir, J., Eldredge, J.D., Aurnou, J.M., 2012. The effects of boundary topography on convection in Earth's core. Geophys. J. Int. 189, 799–814.

Cao, A., Romanowicz, B., 2007. Test of the innermost inner core models using broadband PKIKP travel time residuals. Geophys. Res. Lett. 34, 1–5.

Cormier, V.F., Li, X., 2002. Frequency dependent attenuation in the inner core. 2. A scattering interpretation. J. Geophys. Res. 107, 2374.

Cormier, V.F., Stroujkova, A., 2005. Waveform search for the innermost inner core. Earth Planet. Sci. Lett. 236, 96–105.

Creager, K.C., 1992. Anisotropy of the inner core from differential travel times of the phases PKP and PKIKP. Nature 356, 309–314.

Creager, K.C., 1999. Large-scale variation in inner core anisotropy. J. Geophys. Res. 104, 23127–23139.

Deguen, R., Alboussiere, T., Cardin, P., 2013. Thermal convection in Earth's inner core with phase change at its boundary. Geophys. J. Int. 194, 1310–1334.

Deuss, A., Irving, J.C.E., Woodhouse, J.H., 2010. Regional variation of inner core anisotropy from seismic normal mode observations. Science 328, 1018–1020.

Dziewonski, A.M., Gilbert, F., 1976. The effect of small aspherical perturbations on travel times and a re-examination of the corrections for ellipticity. Geophys. J. R. Astron. Soc. 44, 7–17.

Engdahl, E.R., van der Hilst, R., Buland, R., 1998. Global teleseismic earthquake relocation with improved times and procedures for depth determination. Bull. Seismol. Soc. Am. 88, 722–743.

Garcia, R., 2002. Constraints on upper inner core structure from waveform inversion of core phases. Geophys. J. Int. 150, 651–664.

Gubbins, D., Alfe, D., Davies, C.J., 2013. Compositional instability of Earth's solid inner core. Geophys. Res. Lett. 40, 1084–1088.

Gubbins, D., Sreenivasan, B., Mound, J., Rost, S., 2011. Melting of the Earth's inner core. Nature 473, 361–363.

Irving, J.C.E., Deuss, A., 2011. Hemispherical structure in inner core velocity anisotropy. J. Geophys. Res. 116, 1–17.

Ishii, M., Dziewonski, A.M., 2002. The innermost inner core of the earth: Evidence for a change in anisotropic behaviour at the radius of about 300 km. Proc. Natl. Acad. Sci. USA 99, 14026–14030.

Ishii, M., Dziewonski, A.M., 2005. Constraints on the outer-core tangent cylinder using normal mode splitting measurements. Geophys. J. Int. 162, 787–792.

Karato, S., 1993. Inner core anisotropy due to the magnetic field-induced preferred orientation of iron. Science 262, 1708–1711.

Kennett, B.L.N., Engdahl, E.R., Buland, R., 1995. Constraints on seismic velocities in the Earth from traveltimes. Geophys. J. Int. 122, 108–124.

Li, X., Cormier, V.F., 2002. Frequency-dependent seismic attenuation in the inner core. 1. A viscoelastic interpretation. J. Geophys. Res. 107, 2361–2374.

Li, C., van der Hilst, R.D., Burdick, S., 2008. A new global model for P wave speed variations in Earth's mantle. Geochem. Geophys. Geosyst. 9, 1–21.

Martorell, B., Brodholt, J., Wood, I.G., Vocadlo, L., 2013. The effect of nickel on properties of iron at the conditions of Earth's inner core: Ab initio calculations of seismic wave velocities of Fe–Ni alloys. Earth Planet. Sci. Lett. 365, 143–151.

Mattesini, M., Belonoshko, A., Buforn, E., Ramirez, M., Simak, S., Udias, A., Mao, H., Ahuja, R., 2010. Hemispherical anisotropic patterns of the Earth's inner core. Proc. Natl. Acad. Sci. USA 107, 9507–9512.

Monnereau, M., Calvet, M., Margerin, L., Souriau, A., 2010. Lopsided growth of the Earth's inner core. Science 328, 1014–1017.

Morelli, A., Dziewonski, A.M., Woodhouse, J.H., 1986. Anisotropy of the inner core inferred from PKIKP travel times. Geophys. Res. Lett. 13, 1545–1548.

Niu, F., Chen, Q.F., 2008. Seismic evidence for distinct anisotropy in the innermost inner core. Nat. Geosci. 1, 692–696.

Niu, F., Wen, L., 2001. Hemispherical variations in seismic velocity at the top of Earth's inner core. Nature 410, 1081–1084.

Pozzo, M., Davies, C., Gubbins, D., Alfè, D., 2012. Thermal and electrical conductivity of iron at Earth's core conditions. Nature 485, 355–358.

Sha, X., Cohen, R.E., 2010. First-principles thermal equation of state and thermoelasticity of hcp Fe at high pressures. Phys. Rev. 81, 1–10.

Souriau, A., Testem, A., Chevrot, S., 2003. Is there any structure inside the liquid outer core? Geophys. Res. Lett. 30, 1567.

Steinle-Neumann, G., Stixrude, L., Cohen, R.E., Gulseren, O., 2001. Elasticity of iron at the temperature of the Earth's inner core. Nature 413, 57–60.

Stixrude, L., Cohen, R.E., 1995. High-pressure elasticity of iron and anisotropy of the Earth's inner core. Science 267, 1972–1975.

Su, W., Dziewonski, A., 1995. Inner core anisotropy in 3 dimensions. J. Geophys. Res. 100, 9831–9852.

Sun, X., Song, X., 2008. The inner core of Earth: Texturing of iron crystals from three-dimensional seismic anisotropy. Earth Planet. Sci. Lett. 269, 56–65.

Tanaka, S., 2012. Depth extent of hemispherical inner core from PKP(df) and PKP(Cdiff) for equatorial paths. Phys. Earth Planet. Inter. 210, 50–62.

Tanaka, S., Hamaguchi, H., 1997. Degree one heterogeneity and hemispherical variation of anisotropy in the inner core from PKP(BC)–PKP(DF) times. J. Geophys. Res. 102, 2925–2938.

Vocadlo, L., Dobson, D., Wood, I., 2009. Ab initio calculations of the elasticity of hcp-Fe as a function of temperature at inner-core pressure. Earth Planet. Sci. Lett. 288, 534–538.

Waszek, L., Irving, J., Deuss, A., 2011. Reconciling the hemispherical structure of the Earth's inner core with its super-rotation. Nat. Geosci. 4, 264–267.

Wen, L., Niu, F., 2002. Seismic velocity and attenuation structures in the top if the Earth's inner core. J. Geophys. Res. 107, 2273.

Wessel, P., Smith, W.H.F., 1998. New, improved version of generic mapping tools released. Eos 79, 579.

Woodhouse, J.H., Giardini, D., Li, X.D., 1986. Evidence for inner core anisotropy from free oscillations. Geophys. Res. Lett. 13, 1549–1552.

Yoshida, S., Sumita, I., Kumazawa, M., 1996. Growth model of the inner core coupled with outer core dynamics and the resulting elastic anisotropy. J. Geophys. Res. 101, 28085–28103.